ChemPubSoc Europe

DOI: 10.1002/ejic.201501401

EurJIC European Journal of Inorganic Chemistry

Full Paper

Nitroprussides

Layered Transition Metal Nitroprussides – Their Preparation, Crystal Structure, and Magnetic Properties

Diego Mauricio Gil,[a] Hernandez Osiry,[b] Alejandro Rodriguez,[b] Ana Adela Lemus-Santana,[b] Raúl Ernesto Carbonio,[c] and Edilso Reguera*[b]

Abstract: Divalent transition metal (T) nitroprussides form a series of insoluble coordination compounds, which generally crystallize in 3D frameworks, except for a layered (2D) phase of copper. In this contribution, the preparation of layered phases for T = Mn, Fe, Co, Ni, Zn, and Cd is reported. The incorporation of imidazole (Im) during their preparation by the precipitation method inhibits the coordination of the axial CN groups to the metal T, and layered (2D) structures of formula unit $T(Im)_2[Fe(CN)_5NO]$ result. The metal T is found coordinated to the N end of the equatorial CN groups. Imidazole molecules occupy its axial coordination sites. In the interlayer region, imidazole molecules from neighboring layers interact through their dipole and quadrupole moments. The stacking of the aromatic rings from neighboring molecules deviates from the sandwich-type configuration, which in turn weakens the magnetic interactions between T^{2+} cations located in neighboring layers. Axial unbridged CN and NO groups play a steric hindrance role, thus causing a deviation from the sandwich configuration for the aromatic rings. This series of 2D transition metal nitroprussides can be exfoliated by using appropriate solvents, for example, 1-methyl-2-pyrrolidone.

Introduction

Layered solids (2D) form a large family of materials characterized by stacked sheets held together by physical interactions between the sheets. Within the sheets, the atoms remain linked by covalent bonds. Such sheets can be separated by using physical methods or appropriate solvents to obtain single 2D crystals.[1,2] Probably the most relevant example is the exfoliation of graphite to obtain graphene sheets and the discovery of its unique and fascinating physical properties,[3,4] among them, exceptionally high charge mobility and mechanical stability. Such properties of graphene triggered the interest for 2D materials, and the search for novel layered solids, among them coordination polymers.[5]

The exfoliation of layered solids is the source of large 2D building blocks to prepare 3D porous frameworks by crystal engineering routes, for example, by intercalating pillar species between neighboring layers.[6] From 2D coordination polymers with unsaturated metal centers, the intercalation of organic molecules with nitrogen- or oxygen-donating groups produces 3D porous frameworks of ordered structure (crystalline) with regular pore size and geometry.[7] The functionality of such porous solids for gas storage and separation,[8] as nanoreactor systems,[21] and energy conversion and storage,[9–11] is determined by both the 1D and 2D building blocks, and can be tuned through appropriate selection of these building units. The resulting solids incorporate functionality and flexibility, given by organic materials with the robustness of the inorganic 2D block. From this fact, 3D porous frameworks constructed by the assembly of 2D and 1D building units are able to adapt their pore size and geometry and the available pore volume to the chemical potential and the nature of the species to be adsorbed or released.[12] In addition, the coordination of organic entities at specific and regular distances within the sheets opens up the possibility of studying the intermolecular interactions of molecules confined in a reduced volume. This reduced volume limits the degrees of freedom and minimizes the interference effects of near molecules that exist in the bulk.[13]

The above-mentioned unique properties of 2D solids and their role as sources of 2D building units for crystal engineering, highlights the convenience of having preparative routes to obtain bidimensional materials. Layered materials result from a preferential growth in two dimensions related to the electronic structure of the involved atoms, for example, in graphene, the sp^2 hybridization for the carbon atom. Such materials could also be obtained from building units that usually produce 3D frameworks, once the growth in the axial direction is inhibited. In this contribution, this second option is illustrated for the preparation of layered transition metal nitroprussides. This series of coordination compounds is usually obtained as 3D solids,[14] ex-

[a] Instituto de Química Física, Facultad de Bioquímica, Química y Farmacia, Universidad Nacional de Tucumán, San Lorenzo 456, T4000CAN, San Miguel de Tucumán, Argentina
[b] Centro de Investigación en Ciencia Aplicada y Tecnología Avanzada, Unidad Legaria, Instituto Politécnico Nacional, México, D. F. México
E-mail: edilso.reguera@gmail.com
http://remilab.cicata.ipn.mx
[c] INFIQC - CONICET, Departamento de Físico Química, Facultad de Ciencias Químicas, Universidad Nacional de Córdoba, Haya de la Torre esq. Medina Allende, Ciudad Universitaria, X5000HUA Córdoba, Argentina

Supporting information and ORCID(s) from the author(s) for this article are available on the WWW under http://dx.doi.org/10.1002/ejic.201501401.

cept for a copper(II) phase, which has a layered structure.[15] To obtain layered phases of other metals (Mn, Fe, Co, Ni, Zn, Cd) in the series, the growth along the axial direction was inhibited by using a nitrogen-donor molecule; in this case, we used imidazole as the axial ligand. In the interlayer region, imidazole molecules bonded to adjacent layers interact though their dipole and quadrupole moments, interactions which are of a physical nature, a typical feature of layered solids. The crystal structures for the obtained solids were solved and refined from powder X-ray diffraction patterns (PXRD). The characterization of these materials was completed from spectroscopic and thermal data. The intermolecular interactions in the interlayer region were studied from the refined crystal structures and low-temperature magnetic measurements. To the best of our knowledge, this is the first report on the preparation and study of this series of layered transition metal nitroprussides.

Transition metal pentacyanides, $T[Fe^{III}(CN)_5L]$, where the sixth ligand (L) in the complex anion is different from a nitrosyl group, for example, imidazole and its derivatives, with 2D structures have been reported and studied as prototype bidimensional molecular magnets.[16–18] The results discussed herein are novel in the sense that the sixth ligand (L) is the NO group, which through its unique electronic features, determines the solid structure and physical properties.

Results and Discussion

Spectroscopic and Thermal Characterization

The recorded IR spectra (see the Supporting Information) provide the simplest evidence for the formation of layered phases of the materials under study. These spectra show two bands for the CN stretching mode, with a frequency difference of about 20 cm^{-1}. These two bands correspond to the existence of four equatorial CN groups coordinated at both C and N ends, and to the axial CN ligand unlinked at the N end. The solids formed in the absence of imidazole (3D phases[14]) contain a single CN stretching band, indicating that the five CN groups form bridges between the metal centers. The ν(NO) band is observed at a relatively lower frequency, at about 20 cm^{-1} below the value found for the 3D analogs.[19] Such a frequency shift is due to the layered nature of the formed solid and to the binding of the organic ligand to the axial positions for the metal (T).[20] The IR spectrum also provides definite clues about the imidazole molecule coordination to the metal. A network of hydrogen bonds involving the pyrrolic N–H group and pyridinic nitrogen with the presence of Fermi resonances characterizes molecular solid imidazole, which produces a broad IR absorption in the 3400–2400 cm^{-1} spectral region. On the formation of a coordination bond through the pyridinic nitrogen to form the 2D transition metal nitroprussides, that broad absorption disappears and the ν(N–H) stretching vibration is observed at a higher frequency, at above 3200 cm^{-1}. Table S1 (in the Supporting Information) summarizes the IR bands and assignments of the vibrational modes of imidazole observed in the spectra of the metal complexes. The assignment was performed according to quantum chemical calculations at the B3LYP/6-311++G(d,p) level of approximation. For all complexes, the most important bands related to vibrations of the imidazole are located between 1500 and 400 cm^{-1}, which show small but detectable frequency shifts and intensity changes relative to the free ligand, which reveal the molecule's coordination to the metal (T). The most pronounced changes are observed for the ν(N–H), ν(C–H), δ(N–H), and δ(ring) modes, clearly denoting the extensive delocalization of the negative charge over the ring nitrogen group. The spectrum for the region below 1700 cm^{-1} results from a superposition of bands from the imidazole molecule and those within the nitroprusside ion, δ(FeNO), ν(FeN), $\delta(FeCN)_{eq+ax}$, $\nu(FeC)_{eqA'+A''}$ and $\nu(FeC)_{eqA'}$. The absence of ν(OH) bands corresponding to water molecules indicates the formation of an anhydrous solid, and this suggests that it is free of metal centers with unsaturated coordination sites, which could attach water molecules. Such features differ from the zeolitic behavior of the (3D) solid formed in the absence of the organic ligand, where the presence of both coordinated and hydrogen-bonded water molecules is detected in the IR spectrum (see the Supporting Information). In these 3D solids, the T^{2+} cation has a mixed coordination sphere formed by the N ends of the CN groups and water molecules.[19]

The recorded UV/Vis spectra (see the Supporting Information) support the structural evidence provided by IR spectroscopy. For T = Fe, Co, and Ni, the observed absorption bands in the visible region correspond to d–d transitions in an octahedral environment.[20] These bands are observed at 930, 800, 520, and 480 nm for Fe; 460, 530, and 1040 nm for Co; and 570 and 940 nm for Ni. For the remaining metals (Mn, Zn, Cd), no such transitions are possible because their *n*d electron shell is half filled (Mn) or filled (Zn, Cd). Metal–ligand electronic charge transfers within the nitroprusside ion of the type 11e→13e, 12e→13e, 2b2→13e, and 12e→$4b_1$[21] are observed at lower wavelength. These transitions make evident the metal coordination to the N end of the CN group. A certain spectral shift for their position is observed relative to the bands corresponding to sodium nitroprusside (see the Supporting Information). The charge donation to the metal at the N end of the CN group, through its 5σ orbital, increases the π-back donation from the inner Fe atom and this modifies the energetic states within the complex anion and the related metal–ligand transitions.

The recorded thermogravimetric (TG) curves are free of weight loss below 150 °C, which corresponds to an anhydrous solid (see the Supporting Information). This is in agreement with the results from the IR spectra, which are free of ν(OH) and δ(H-O-H) bands. The TG curve for $Cd(Im)_2[Fe(CN)_5NO]$ exhibits a smooth weight loss at around 100 °C, indicating the presence of a hydrated 3D phase as an impurity, which was confirmed by PXRD (see below). From that temperature onward, three thermal effects are detected; according to the weight loss, the first two (unresolved for Zn) correspond to the evolution of two imidazole molecules plus the unbridged CN and NO groups. These are unbridged species and from this fact, their evolution on heating is observed at relatively a low temperature.[22] Then, at higher temperatures, the decomposition of the metal complex salt is completed with the evolution of the equatorial CN ligands, and formation of metallic species or metal oxides, de-

pending on the experiment atmosphere, that is, non-oxidizing or oxidizing, respectively. The formation of metallic species is related to the reducing character for the evolved cyanide radicals.[23]

Crystal Structure

The 2D solids under study crystallize with an orthorhombic unit cell in the $P2_12_12_1$ space group. For T = Co, Ni, the unit cell accommodates four formula units (Z = 4) but for Mn, Fe, Zn, and Cd the cell practically has double volume and it is occupied by eight formula units (Z = 8). Figure 1 shows the PXRD pattern and its fitting according to the structural model for T = Mn. Analog pattern fits were obtained for the remaining metals (see the Supporting Information). Table 1 collects the cell parameters for the six compositions of this series of 2D solids. According to the cell volume, for Co and Ni, the solids crystallize with a less compact structure; compared with Mn, Fe, Zn, and Cd, their formula unit occupies about 10 % greater volume. The nature of such behavior is related to intermolecular interactions in the interlayer region (discussed below). The refined crystal structures have physical meaning and are in accordance with the spectroscopic information discussed above. Figures 2 and 3 show the atomic packing within the unit cell for the series. In the interlayer region, imidazole molecules from neighboring layers interact through their dipole and quadrupole moments. Imidazole is a molecule with dipole (**p**) and quadrupole (**Q**) moments: **p** = 3.87 D, and Q_{xx} = –23.14, Q_{yy} = –30.10, and Q_{zz} = –32.47 D·Å.[13] In the interlayer region, the relative orientation

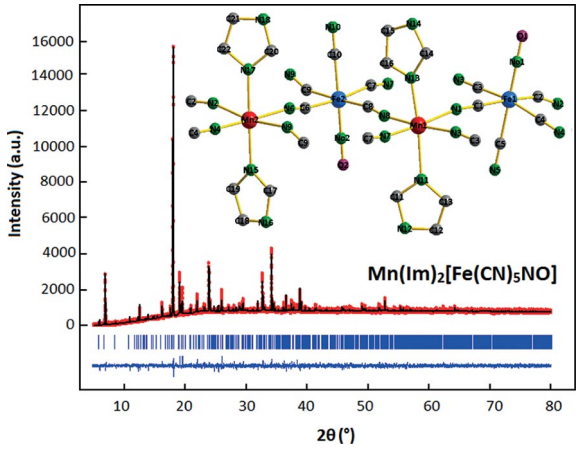

Figure 1. Experimental PXRD pattern and its fitting according to the refined structural model for $Mn(Im)_2[Fe(CN)_5NO]$. Inset: Coordination environments for the involved metals (labels: Fe: blue sphere; Mn: red sphere).

Table 1. Unit cell parameters and cell volume for the series $T(Im)_2[Fe(CN)_5NO]$.

Metal (T)	Unit cell parameters [Å]	Z value and cell volume [Å^3]	Cell volume per formula unit [Å^3]
Mn	a = 29.5581(2); b = 14.0789(4); c = 7.4283(2)	Z = 8 3091.25(12)	386.41
Fe	a = 29.1508(1); b = 13.9651(1); c = 7.3492(2)	Z = 8 2991.81(8)	373.98
Co	a = 16.0188(3); b = 14.3827(1); c = 7.44602(8)	Z = 4 1715.51(19)	428.88
Ni	a = 15.7738(3); b = 14.4547(2); c = 7.2792(1)	Z = 4 1659.7(5)	414.93
Zn	a = 29.2527(2); b = 14.0263(1); c = 7.3187(4)	Z = 8 3002.92(17)	375.36
Cd	a = 30.2566(7); b = 14.0242(3); c = 7.5462(2)	Z = 8 3202.04(13)	400.26

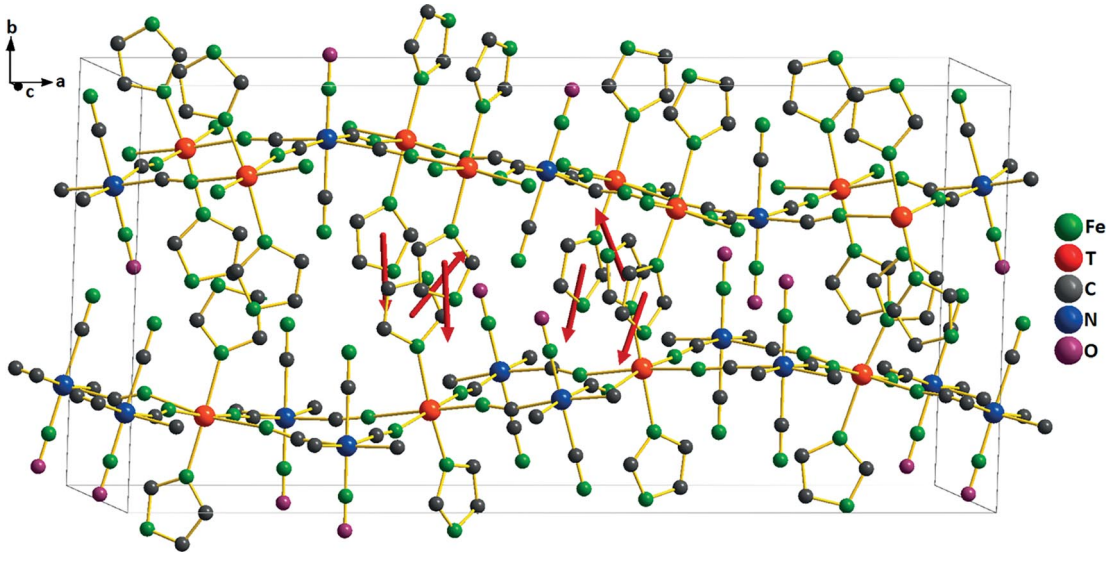

Figure 2. Atomic packing within the unit cell of $T(Im)_2[Fe(CN)_5NO]$ with T = Mn, Fe, Zn, Cd. The red arrows indicate the molecules' dipole moments.

for the dipole moment from neighboring molecules is antiparallel, which corresponds to their attractive coupling. Such interactions, which are of a physical nature, support the material's 3D framework. This is a feature for layered solids, in which neighboring sheets are held together through forces of a physical nature. These electrostatic interactions and steric factors determine the undulating configuration observed for the layers. For 2D copper nitroprusside dihydrate, which has relatively weak intermolecular interactions in the interlayer region, the sheets adopt a flat (planar) configuration.[15]

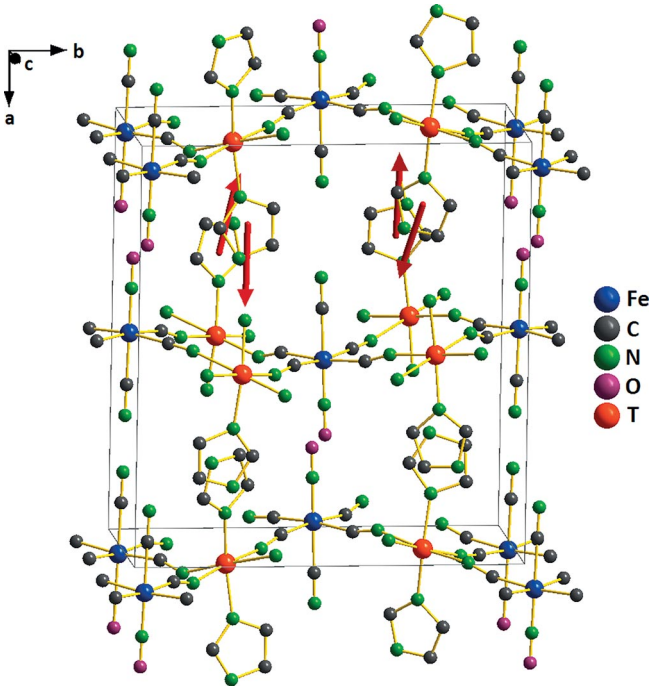

Figure 3. Atomic packing within the unit cell of $T(Im)_2[Fe(CN)_5NO]$ with T = Co, Ni. The red arrows indicate the molecules' dipole moments.

The refined atomic positions, occupancies, and thermal factors, the calculated bond lengths and angles are available in the Supporting Information. The structural information, including CIF files, was deposited with the Cambridge Crystallographic Data Centre (see below). According to the refined crystal structures, the coordination geometry for the T atom is octahedral; the imidazole molecules occupy its axial coordination sites. This explains the anhydrous character for these solids. The coordination polyhedra for both the inner (Fe) and outer (T) metals are distorted octahedra, which are related to the nature of their ligands, and this contributes to the serpentine configuration for the layers. The energy splitting in the t_{2g} levels of the T^{2+} cation that originates from the octahedral distortion remains below kT at room temperature, as suggested by the magnetic measurements (discussed below). Table 2 summarizes the relevant bond and ring–ring distances and angles for the series of layered solids under study. The T–N_{Im} distance follows a positive correlation with the metal polarizing power (Ze/r^2).[24] For the most polarizing metal in the series (Ni), the smallest cell volume and the shortest T–N_{Im} distance were observed. The polarizing power parametrizes the metal ability to subtract charge from the ligand.

Table 2. Relevant interatomic distances and angles for the series $T(Im)_2[Fe(CN)_5NO]$.

Metal	Polarizing power (Ze/r^2)[a]	T–N_{Im}, [Å]	Ring–ring distance [Å]	Ring–ring angle [°]
Mn	3.287	Mn_1–N_{11}: 2.237(7) Mn_1–N_{13}: 1.987(9) Mn_2–N_{15}: 2.082(7) Mn_2–N_{17}: 2.146(7)	3.727(1)–3.773(1)	171.4–173.9
Fe	3.463	Fe_3–N_{11}: 1.959(10) Fe_3–N_{13}: 1.922(10) Fe_4–N_{15}: 1.923(11) Fe_4–N_{17}: 1.927(10)	3.558(4)–3.699(5)	162.6–175.2
Zn	3.652	Zn_1–N_{11}: 2.696(9) Zn_1–N_{13}: 2.520(10) Zn_2–N_{15}: 2.089(8) Zn_2–N_{17}: 2.573(8)	3.200(3)–3.817(4)	163.3–173.5
Cd	2.041	Cd_1–N_{11}: 2.737(10) Cd_1–N_{13}: 2.158(11) Cd_2–N_{15}: 2.135(11) Cd_2–N_{17}: 2.269(9)	3.712(5)–4.065(4)	152–176.9
Co	3.652	Co–N_6: 2.103(10) Co–N_8: 2.034(19)	4.070(4)	142.1
Ni	3.858	Ni–N_6: 2.070(9) Ni–N_8: 1.999(10)	3.778(4)	158.2

[a] The values of polarizing power were taken from reference.[24]

In the interlayer region, the ring–ring angle for neighboring imidazole molecules deviates from the coplanar (sandwich) configuration; without exception, the ring–ring angle remains below 180°. For the thiazole and imidazole and their derivatives intercalated between $T[Ni(CN)_4]$ layers, a sandwich-type configuration has been observed.[13,25] Likely, the deviation from coplanar arrangement for the herein studied series of 2D solids is related to steric factors, which in turn are determined by the presence of the unbridged CN and NO ligands in the axial positions of Fe. This also accounts for the relatively large variation observed for the ring–ring distance, calculated from the center to center of the rings, except for Co and Ni (see Table 2). In the crystal structure for these last two metals, adjacent layers are accommodated within a higher available cell volume and this probably minimizes the steric impediments and favors a smaller ring–ring distance. The calculated ring–ring distances for all the series are in the limit of distance required for a π–π interaction to be favorable and to allow for a magnetic coupling between T metals from neighboring layers. For imidazole that distance is 3.70 Å.[13]

Intermolecular Interactions and Magnetic Properties

In the series of 2D materials under study, for T = Mn, Fe, Co, and Ni, two types of magnetic interactions are possible between the T^{2+} cations. The Fe^{II} ion in the nitroprusside building block remains in a low spin state and its contribution to the magnetic properties is of diamagnetic nature. Within the layer $T[Fe(CN)_5NO]$, the interaction between T metals at distances above 10 Å, is expected to be of antiferromagnetic nature because it corresponds to equal ions coupled through the 5σ orbitals of CN groups in the –N≡C–Fe–C≡N– chain. The interaction is expected to have ferromagnetic character through the over-

lapping of π clouds from neighboring imidazole molecules. Such dual behavior has been registered for $T(DIm)_2[Ni(CN)_4]$ solids where T is a transition metal, and DIm is imidazole and its derivatives.[13] As already mentioned, neighboring molecules in the interlayer region remain coupled through dipolar and quadrupolar forces, which makes possible the antiparallel stacking of their aromatic rings. When the ring–ring distance remains below 3.70 Å, a ferromagnetic interaction between neighboring T metals from different layers is expected.[13] The unpaired electrons in the metals, available for the magnetic interaction, reside in their 3d orbitals and super exchange magnetic coupling takes place through the imidazole molecules' π-clouds. Both the antiferromagnetic and ferromagnetic interactions are relatively weak and could be observed only at low temperature.

Figure 4 shows the temperature dependence for the $\chi_M T$ curve for the $T(Im)_2[Fe(CN)_5NO]$ series with T = Mn, Fe, Co, Ni. The values of effective magnetic moment (μ_{eff}) were calculated according to $\mu_{eff} = 2.828\ (\chi_M T)^{1/2}$ and by introducing the appropriate diamagnetic correction.[26] The temperature dependence for the values of μ_{eff} is available in the Supporting Information. Table 3 summarizes the experimental μ_{eff} values at room temperature, and the expected ones in the absence and presence of spin–orbit coupling. The values of μ_{eff} at room temperature could be interpreted as resulting from spin-only contributions, except for Co^{2+} and Fe^{2+}. For these last two cations, the temperature dependence for the value of μ_{eff}, and of course of $\chi_M T$, is a conclusive clue for the presence of spin–orbit coupling; on cooling, a progressive decrease in the value of μ_{eff} is observed (see the Supporting Information). For Fe^{2+} and Co^{2+} in an octahedral coordination environment, the t_{2g} orbitals accommodate four and five electrons, respectively, resulting a degenerate energy system (the three t_{2g} orbitals have the same energy). These electrons have the same probability of occupying the three orbitals and from this fact results the spin–orbit coupling observed for these ions in an octahedral crystal field. For the materials under study, the T^{2+} ion is found to have a distorted coordination environment. The appearance of spin–orbit coupling effects for Fe^{2+} and Co^{2+} suggests that the thermal energy kT is enough to preserve the degeneration in their t_{2g} orbitals; the value of kT at intermediate and room temperature is higher than the energy splitting of these orbitals, which originates from the distortion of the coordination polyhedron. This explains why at low temperature the value of μ_{eff} is close to the expected one in the absence of spin–orbit coupling, except in the temperature region where a cooperative interaction appears (see the Supporting Information). For Mn^{2+} and Ni^{2+} the appearance of spin–orbit coupling is only possible for mixed ground and excited states, but no evidence of such effects was observed for these two cations. For Mn at low temperature, the value of μ_{eff} shows a slight increase corresponding to a weak (incipient) ferromagnetic interaction.

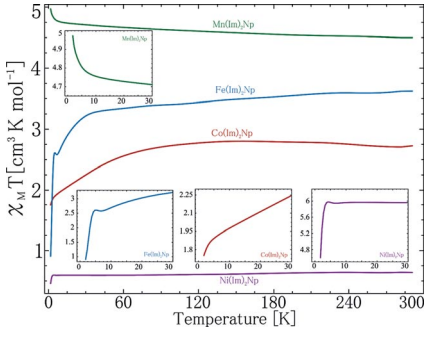

Figure 4. Temperature dependence for $\chi_M T$ in the $T(Im)_2[Fe(CN)_5NO]$ series. Insets: Expansion of the low-temperature region of the $\chi_M T$ curves to illustrate the appearance of an incipient (quite weak) ferromagnetic interaction through π–π coupling of neighboring imidazole molecules.

Table 3. Magnetic susceptibility values (in Bohr magneton units) at room temperature (300 K) for $T(Im)_2[Fe(CN)_5NO]$ and the calculated Curie–Weiss constant (θ_{CW}).

Metal (T^{2+})	Exp. value	Expected value[a] (spin+orbital)	Expected value[a] (spin only)	Unpaired electrons	θ_{CW} [K]
Mn^{2+}	6.02	5.90	5.92	5 e^-	0.31
Fe^{2+}	5.35	5.1–5.5	4.9	4 e^-	–2.63[b]
Co^{2+}	4.66	4.1–5.2	3.87	3 e^-	–1.50
Ni^{2+}	2.93	2.8–4.0	2.83	2 e^-	–0.16

[a] Taken from reference.[28] [b] In the paramagnetic region.

The temperature dependence for the value of $\chi_M T$ below 30 K in the solids containing Fe^{2+} and Co^{2+} suggests the presence of certain contributions from the zero-field splitting (ZFS) effect to the magnetic properties. For these two cations, below 30 K, the value of $\chi_M T$ shows a practically parabolic decrease, a typical feature in the presence of ZFS effects. The ZFS parameters (D, E) for Co^{2+} were estimated from the magnetization curves versus applied magnetic field at different temperatures by using PHI software (see the Supporting Information).[27] The obtained values for these parameters for Co^{2+} were D = 2.91 cm^{-1}, E = 0.01 cm^{-1}. The value of D dominates the ZFS effect, which is related to the axial distortion for the T^{2+} cation coordination polyhedron. The values found for D and E are similar to those reported for these paramagnetic ions diluted in diamagnetic matrix and in the presence of negligible interactions between neighboring paramagnetic centers.[28] For Fe, the presence of a weak ferromagnetic interaction at low temperature limited the ZFS parameters calculation. At higher temperatures, the ZFS effect could also be present but it appears mixed with the spin–orbit coupling and all efforts to obtain reliable ZFS parameters for that region failed.

For Fe^{2+} at low temperature, a definite ferromagnetic ordering was observed (Figure 4, inset). From 6 K, on cooling, the values of $\chi_M T$ shows a sudden increase corresponding to the appearance of a cooperative interaction of ferromagnetic nature involving Fe^{2+} ions located in neighboring layers, followed of a pronounced decrease, which was ascribed to the antiferromagnetic interaction between T metals within the layer. That weak ferromagnetic interaction takes place through the π-clouds overlapping from neighboring imidazole molecules. This magnetic behavior at low temperature is supported by the refined crystal structure for $Fe(Im)_2[Fe(CN)_5NO]$, and it is consistent with previous studies on imidazole intercalation in layered solids.[13] The calculated ring–ring distance (Table 2) remains below the limit value of 3.70 Å required to observe the magnetic interaction through π–π stacking in imidazole and its derivatives.[13] For Ni^{2+}, such an interaction is practically imperceptible

tible and it is responsible for a slight increase in the $\chi_M T$ curve close to 2 K. For Mn^{2+}, the increase on cooling is more pronounced, which is probably related to the high spin density of this ion (S = 5/2). No evidence of ferromagnetic interactions was observed for Co^{2+}. For the solid containing Mn^{2+}, the Curie–Weiss constant (θ_{CW}) is slightly positive (0.31 K), corresponding to a weak ferromagnetic interaction but, for Co^{2+}, Ni^{2+}, and Fe^{2+} (> 6 K), it is slightly negative, indicating that the interaction is dominated by the weak antiferromagnetic coupling of neighboring paramagnetic centers within the layer. The values found for θ_{CW} are included in Table 3. The magnetization curve versus applied magnetic field at 2 K for $Fe(Im)_2[Fe(CN)_5NO]$ is available in the Supporting Information. A narrow but definite hysteresis loop was observed, in correspondence with the evidence obtained from the low-temperature behavior for the effective magnetic moment. In the AC susceptibility curve (see the Supporting Information), only a slight inflection below 5 K is detected, which suggests that the magnetic coupling detected in the $\chi_M T$ versus T curve is quite weak.

Layered Solid Exfoliation

The studies related to the physical properties of graphene have illustrated the importance of having appropriate methods to exfoliate layered solids to obtain information about the properties of their individual sheets. Such possibilities were explored for the series of 2D transition metal nitroprussides under study. The exfoliation was carried out in an ultrasound bath by using 1-methyl-2-pyrrolidone (1m2p) as the solvent. This is a solvent with a high surface tension (γ), over 40 mJ m^{-2}, which minimizes the required exfoliation energy.[1,2] Samples of $T(Im)_2[Fe(CN)_5NO]$ were added to a glass vessel containing 1m2p and then submitted to ultrasound for 10 to 30 min. Initially, the layered solid appears as a powder in the bottom of the vessel, but on treatment with ultrasound, a cloudy suspension is formed, which remains stable for many days but finally precipitates through interaction of the solvent molecules with the layers. The UV/Vis spectra of that cloudy suspension and of the exfoliated precipitate are similar to each other and also to the initial solid, except for a redshift for the d–d transitions in the cases of Fe^{2+}, Co^{2+}, and Ni^{2+} (see the Supporting Information). This redshift was ascribed to changes in the metal (T) coordination environment in the absence of intermolecular interactions. No appreciable changes were observed for the metal–ligand charge-transfer bands. Such spectral evidence suggests that the solid is exfoliated with preservation of the sheet integrity. The IR spectra for the exfoliated solids are similar to the ones obtained for the original 2D materials (see the Supporting Information). These experimental results are conclusive clues to the feasibility of exfoliation for layered transition metal nitroprussides.

Conclusions

Layered divalent transition metal nitroprussides were prepared by adding an aqueous solution of the metal salt to a solution containing imidazole and sodium nitroprusside. Imidazole inhibits metal coordination to the axial cyanide group of the nitroprusside complex anion. The axial coordination positions for the metal are occupied by the imidazole molecules. In the interlayer region, imidazole molecules from neighboring sheets interact through their dipole and quadrupole moments, which are forces of a physical nature. These interactions can be disrupted by using an appropriate solvent, for example, 1-methyl-2-pyrrolidone, to exfoliate the 2D solid into individual sheets, which maintain their integrity. As the net electrostatic interaction between neighboring molecules is attractive, their π-clouds partially overlap, which contributes to the stability of the 3D framework through dispersive-type forces. Such π-cloud overlap makes possible the magnetic interactions between T^{2+} cations located in neighboring layers, if the ring–ring distance remains below 3.70 Å. Within the series, this condition is satisfied only for the iron-containing solid and this leads to a ferromagnetic interaction at close to 2 K. For Mn^{2+} and Ni^{2+} at close to 2 K, an incipient (quite weak) ferromagnetic interaction was also detected, related to their high spin density. For Fe^{2+} and Co^{2+}, definite spin–orbit coupling and ZFS effects were observed.

Experimental Section

General: Layered phases of divalent transition metal nitroprussides were obtained by the precipitation method, by mixing aqueous solutions of sodium nitroprusside, imidazole, and of the nitrate of the involved transition metal (T = Mn, Fe, Co, Ni, Zn, or Cd) in the appropriate molar ratio. The formed precipitate was aged for a week in the darkness within the mother liqueur. The resulting precipitates were separated by centrifugation and then washed several times with deionized water to obtain a filtrate free of the accompanying ions. The resulting pasty solid was finally dried at ambient conditions until it had constant weight. The nature of the obtained powder as layered transition metal nitroprussides was established by structural analysis from PXRD data complemented by spectroscopic (IR, UV/Vis) and thermogravimetric (TG) techniques. The formed layered solids, $T(Im)_2[Fe(CN)_5NO]$, were exfoliated by using 1-methyl-2-pyrrolidone, a solvent widely used for graphene and graphene-like exfoliation.[1,2]

PXRD patterns were recorded with Cu-$K_{\alpha 1}$ radiation in the Bragg–Brentano geometry by using a D8 Advance diffractometer (from Bruker) equipped with a Lynx eye detector and germanium monochromator. The DICVOL method[29] was used to index the PXRD pattern and to identify the unit cell. The diffraction patterns were decomposed, in term of extracted intensities, by the Le Bail procedure by using a pseudo-Voigt peak profile function.[30] The background was modeled by a third-order polynomial. Peak profiles were calculated within ten times the full width at half maximum. The structural model to be refined was obtained by a combination of heavy atom and direct methods available in the SHELXs software.[31] The structural model was completed by analysis of the electron density Fourier maps. The structural model was finally refined by using the Rietveld method implemented in the FullProf program.[32] The interatomic C–N, Fe–C, N–O, and Fe–N_{NO} distances were constrained to take values within certain limits by considering the reported crystal structures for 3D transition metal nitroprussides.[19] Additional details of the PXRD data recording and processing procedures are available in the Supporting Information.

TG and differential thermal analysis (DTA) curves were collected in the HR mode under a N_2 flow (0.1 L min^{-1}) by using a TA Instru-

ments (IR-5000) equipment. IR and UV/Vis spectra were recorded by the ATR and integration sphere method, respectively, by using Perkin–Elmer equipment. The low-temperature zero-field cooling/field cooling (ZFC/FC) curves were collected with a MPMS-3 SQUID magnetometer from Quantum Design. The FC curve was recorded under an applied magnetic field of 50 Oe. The magnetization curves versus applied magnetic field were recorded at 2 K in the –6 to 6 T range.

CCDC 1401186 (for $Mn(Im)_2[Fe(CN)_5NO]$), 1401187 (for $Fe(Im)_2[Fe(CN)_5NO]$), 1401190 (for $Co(Im)_2[Fe(CN)_5NO]$), 1401191 (for $Ni(Im)_2[Fe(CN)_5NO]$), 1401188 (for $Zn(Im)_2[Fe(CN)_5NO]$), and 1401189 (for $Cd(Im)_2[Fe(CN)_5NO]$) contain the supplementary crystallographic data for this paper. These data can be obtained free of charge from The Cambridge Crystallographic Data Centre.

Supporting Information (see footnote on the first page of this article): Supplementary spectroscopic, magnetic, and structural information associated with this article.

Acknowledgments

This study was supported by the Mexican Consejo Nacional de Ciencia y Tecnología (CONACyT) (project numbers 2011-01-174247, 2011-01-166387, and SRE-2013-191089). R. E. C. thanks ANPCYT for an international cooperation project (PICT 2012-3079).

Keywords: Layered compounds · Intermolecular interactions · Magnetic properties · Coordination modes · Metal nitroprussides

[1] J. N. Coleman, M. Lotya, A. O'Neill, S. D. Bergin, P. J. King, U. Khan, K. Young, A. Gaucher, S. De, R. J. Smith, I. V. Shvets, S. K. Arora, G. Stanton, H.-Y. Kim, K. Lee, G. T. Kim, G. S. Duesberg, T. Hallam, J. J. Boland, J. J. Wang, J. F. Donegan, J. C. Grunlan, G. Moriarty, A. Shmeliov, R. J. Nicholls, J. M. Perkins, E. M. Grieveson, K. Theuwissen, D. W. McComb, P. D. Nellist, V. Nicolosi, *Science* **2011**, *331*, 568–571.
[2] Y. Hernandez, V. Nicolosi, M. Lotya, F. M. Blighe, Z. Sun, S. De, I. T. McGovern, B. Holland, M. Byrne, Y. K. Gun'Ko, J. J. Boland, P. Niraj, G. Duesberg, S. Krishnamurthy, R. Goodhue, J. Hutchison, V. Scardaci, A. C. Ferrari, J. N. Coleman, *Nature Nanotechnol.* **2008**, *3*, 563–568.
[3] S. Z. Butler, S. M. Hollen, L. Cao, Y. Cui, J. A. Gupta, H. R. Gutiérrez, T. F. Heinz, S. S. Hong, J. Huang, A. F. Ismach, E. Johnston-Halperin, M. Kuno, V. V. Plashnitsa, R. D. Robinson, R. S. Ruoff, S. Salahuddin, J. Shan, L. Shi, M. G. Spencer, M. Terrones, W. Windl, J. E. Goldberger, *ACS Nano* **2013**, *4*, 2898–2913.
[4] C. N. R. Rao, K. Biswas, K. S. Subrahmanyam, A. Govindaraj, *J. Mater. Chem.* **2009**, *19*, 2457–2469.
[5] A. A. Lemus-Santana, M. González, J. Rodríguez-Hernández, M. Knobel, E. Reguera, *J. Phys. Chem. A* **2013**, *117*, 2400–2407.
[6] a) J. T. Culp, S. Natesakhawat, M. R. Smith, E. Bittner, C. Matranga, B. Bockrath, *J. Phys. Chem. C* **2008**, *112*, 7079–7083; b) J. T. Culp, C. Madden, K. Kauffman, F. Shi, C. Matranga, *Inorg. Chem.* **2013**, *52*, 4205–4216.
[7] A. Hazra, P. Kanoo, T. K. Maji, *Chem. Commun.* **2011**, *47*, 538–540.
[8] Z. H. Xuan, D. S. Zhang, Z. Chang, T. L. Hu, X. H. Bu, *Inorg. Chem.* **2014**, *53*, 8985–8990.
[9] N. A. Chernova, M. Roppolo, A. C. Dillon, M. S. Whittingham, *J. Mater. Chem.* **2009**, *19*, 2526–2552.
[10] P. G. Hoertz, T. E. Mallouk, *Inorg. Chem.* **2005**, *44*, 6828–6840.
[11] B. Chen, S. Ma, F. Zapata, F. R. Fronczek, E. B. Lobkovsky, H. C. Zhou, *Inorg. Chem.* **2007**, *46*, 1233–1236.
[12] S. Bureekaew, S. Shimomura, S. Kitagawa, *Sci. Technol. Adv. Mater.* **2008**, *9*, 014108.
[13] a) M. González, A. A. Lemus-Santana, J. Rodríguez-Hernández, M. Knobel, E. Reguera, *J. Solid State Chem.* **2013**, *197*, 317–322; b) M. González, A. A. Lemus-Santana, J. Rodríguez-Hernández, C. I. Aguirre-Vélez, M. Knobel, E. Reguera, *J. Solid State Chem.* **2013**, *204*, 128–135.
[14] E. Reguera, A. Dago, A. Gomez, J. Fernandez-Bertrán, *Polyhedron* **1996**, *15*, 3139–3145.
[15] A. Gómez, J. Rodríguez-Hernández, E. Reguera, *J. Chem. Crystallogr.* **2004**, *34*, 893–903.
[16] R. Lescezec, L. M. Toma, J. Vaissermann, M. Verdaguer, F. S. Delgado, C. Ruiz-Pérez, F. Lloret, M. Julve, *Coord. Chem. Rev.* **2005**, *249*, 2691–2729; and references cited therein.
[17] H. Tchouka, A. Meetsma, W. R. Browne, *Inorg. Chem.* **2010**, *49*, 10557–10570.
[18] C.-C. Zhao, W.-W. Ni, J. Tao, A.-L. Cui, H.-Z. Kou, *CrystEngComm* **2009**, *11*, 632–637.
[19] a) D. B. Mullica, D. F. Tippin, E. L. Sappenfield, *Inorg. Chim. Acta* **1990**, *174*, 129–135; b) D. B. Mullica, D. F. Tippin, E. L. Sappenfield, *J. Crystallogr. Spectrosc. Res.* **1991**, *21*, 81–85; c) D. B. Mullica, D. F. Tippin, E. L. Sappenfield, *J. Coord. Chem.* **1991**, *24*, 83–91; d) D. B. Mullica, D. F. Tippin, E. L. Sappenfield, *J. Coord. Chem.* **1992**, *25*, 175–182.
[20] H. Osiry, A. Cano, A. A. Lemus-Santana, A. Rodríguez, R. E. Carbonio, E. Reguera, *J. Solid State Chem.* **2015**, *230*, 374–380.
[21] P. T. Manoharan, H. B. Gray, *J. Am. Chem. Soc.* **1965**, *87*, 3340–3348.
[22] A. Cano, H. Osiry, L. Reguera, A. A. Lemus-Santana, E. Reguera, *J. Solid State Chem.* **2015**, *225*, 315–320.
[23] R. Robinette, R. L. Collins, *J. Coord. Chem.* **1974**, *4*, 65–70.
[24] Y. Zhang, *Inorg. Chem.* **1982**, *21*, 3886–3889.
[25] F. Echevarría, A. A. Lemus-Santana, M. González, J. Rodríguez-Hernández, E. Reguera, *Polyhedron* **2015**, *95*, 75–80.
[26] O. Khan, *Molecular Magnetism*, VCH Publishers, New York, **1993**.
[27] N. F. Chilton, R. P. Anderson, L. D. Turner, A. Soncini, K. S. Murray, *J. Comput. Chem.* **2013**, *34*, 1164–1175.
[28] R. L. Carlin, *Magnetochemistry*, Springer-Verlag, Berlin, **1986**.
[29] D. Louer, R. Vargas, *J. Appl. Crystallogr.* **1982**, *15*, 542–545.
[30] A. L. Le Bail, *ESPOIR: A Program for Solving Structures by Monte Carlo from Powder Diffraction Data*, in: EPDIC-7, Barcelona, Spain, **2000**, http://www.ccp14.ac.uk/solution/powder_struct_solution/.
[31] G. M. Sheldrick, *Program for Crystal Structure Determination*, University of Göttingen, Germany, **1997**.
[32] J. Rodríguez-Carvajal, *FullProf 2005 Program*, Institute Louis Brillouin, Saclay, France, **2005**.

Received: December 1, 2016
Published Online: March 11, 2016

